INL/CON-11-23634
PREPRINT

Daily Thermal Predictions of the AGR-1 Experiment with Gas Gaps Varying with Time

ICAPP '12

Grant Hawkes
James Sterbentz
John Maki
Binh Pham

June 2012

The INL is a
U.S. Department of Energy
National Laboratory
operated by
Battelle Energy Alliance

Proceedings of ICAPP '12
Chicago, USA, June 24-28, 2012
Paper 12111

Daily Thermal Predictions of the AGR-1 Experiment With Gas Gaps Varying with Time

Grant Hawkes, James Sterbentz, John Maki, Binh Pham
Idaho National Laboratory
2525 Fremont, MS 3870
+1 (208) 526-8767 Grant.Hawkes@inl.gov

Abstract – *A new daily as-run thermal analysis was performed at the Idaho National Laboratory on the Advanced Gas Reactor (AGR) test experiment number one at the Advanced Test Reactor (ATR). This thermal analysis incorporates gas gaps changing with time during the irradiation experiment. The purpose of this analysis was to calculate the daily average temperatures of each compact to compare with experimental results. Post irradiation examination (PIE) measurements of the graphite holder and fuel compacts showed the gas gaps changed from the beginning of life. The control temperature gas gap and the fuel compact – graphite holder gas gaps were modeled with a linear change from the original fabrication gap dimensions to the end of irradiation measurements. A steady-state thermal analysis was performed for each daily calculation with the commercial finite element heat transfer code ABAQUS. These new thermal predictions more closely match the experimental data taken during the experiment than previous analyses. Results are presented comparing normalized compact average temperatures to normalized log(R/B) Kr-85m. The R/B term is the measured release rate divided by the predicted birth rate for the isotope Kr-85m. Correlations between these two normalized values are presented.*

I. INTRODUCTION

A daily as-run thermal analysis has been performed on the advanced gas-cooled reactor (AGR) experiment (AGR-1) in the Advanced Test Reactor (ATR). Six capsules were analyzed for each day of the experiment as discussed in Ref [1]. This paper discusses the daily average, time average volume average temperatures, and the normalized temperatures as a function of irradiation time known as effective full power days (EFPD).

Several fuel and material irradiation experiments, which support the development of the Next Generation Nuclear Plant (NGNP), are planned for the Advanced Gas Reactor Fuel Development and Qualification Program. The goals of these experiments are: to: provide irradiation performance data to support fuel process development, qualify fuel for normal operating conditions, support development and validation of fuel performance and fission product transport models and codes, and provide irradiated fuel and materials for post-irradiation examination and safety testing. AGR-1 was the first in this series of planned experiments to test tri-isotropic (TRISO)-coated, low-enriched uranium oxycarbide fuel. The AGR-1 experiment was intended to serve as a shakedown test of the multiple capsule test train designs to be used in subsequent irradiations and to test early variants of the fuel produced under this program.

The AGR-1 experiment is comprised of six individual capsules, approximately 0.034925 m diameter by 0.1524 m long, stacked on top of each other to form the test train. Each capsule contains 12 fueled compacts that are approximately 0.0127 m diameter by 0.0254 m long. The compacts are composed of fuel particles bound together by a carbon matrix. Each compact contains approximately 4,150 fissile particles (35 vol% particle packing fraction). Each capsule is supplied with a flowing helium/neon gas mixture to control the test temperature and sweep any fission gases that are released to the fission product monitoring system. Temperature control is accomplished by adjusting the gas mixture ratio of the two gases (helium and neon) with differing thermal conductivities.

Each capsule has a different control gas gap designed to control the temperature of each individual capsule. A sensitivity study [2] was performed for the various input parameters. This study showed that the control gas gaps, and fuel compact heat rates affected the thermal results the very most. The finite element stress and heat transfer code ABAQUS in Ref [3] was used to perform the thermal analysis.

The AGR-1 experiment was placed in the B-10 position in the ATR core as shown in Fig 1. Each capsule contains a graphite holder with three equally spaced fuel compact holder openings as shown in Fig 2. Each holder opening accommodates four axially stacked fuel compacts. Thus, each capsule has three stacks by four fuel compacts

per stack for a total of 12 fuel compacts per capsule, with the entire AGR 1 experiment capsule assembly having six capsules by 12 fuel compacts per capsule for a total of 72 fuel compacts.

Fig 3 shows the axial arrangement for Stack-1. The ABAQUS model has a direct volume-for-volume correlation with the physics model discussed in Reference [4] for the heating of the compacts (each compact is evenly axially divided into two equal parts). An axial cut of a typical capsule is shown in Figure 4.

II. MODEL DESCRIPTION

Figures 5 through 9 are used in the description of the model. The finite element mesh is discussed first, followed by a description of the material properties, and ending with the volumetric heat rates imposed on the model

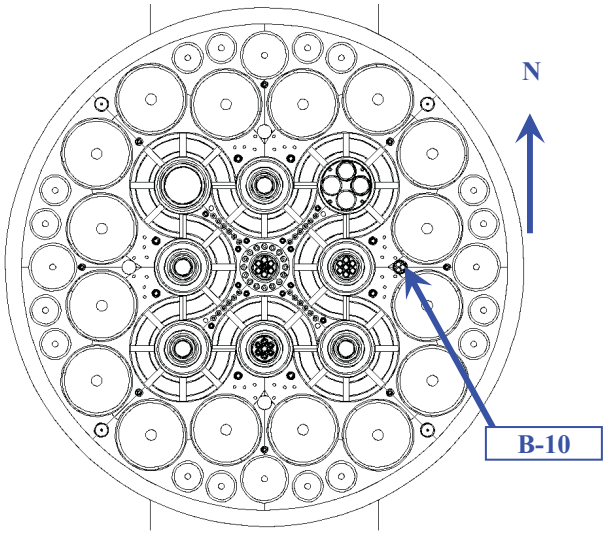

Fig 1. Cross section view of the ATR core, B-10 irradiation test position.

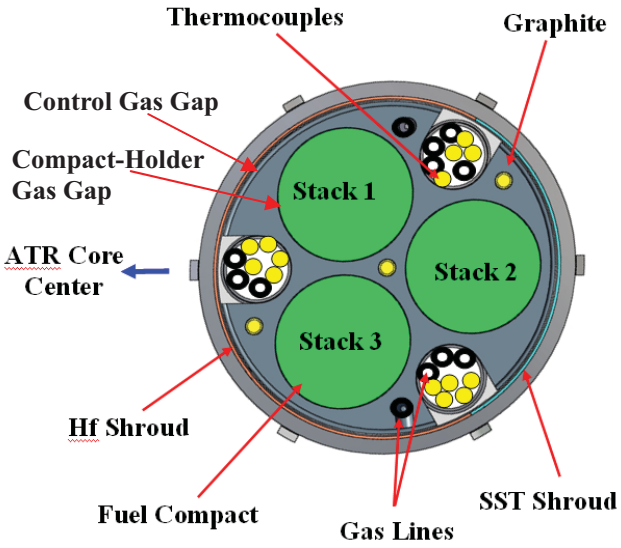

Fig 2. Schematic of cross section of an AGR-1 capsule.

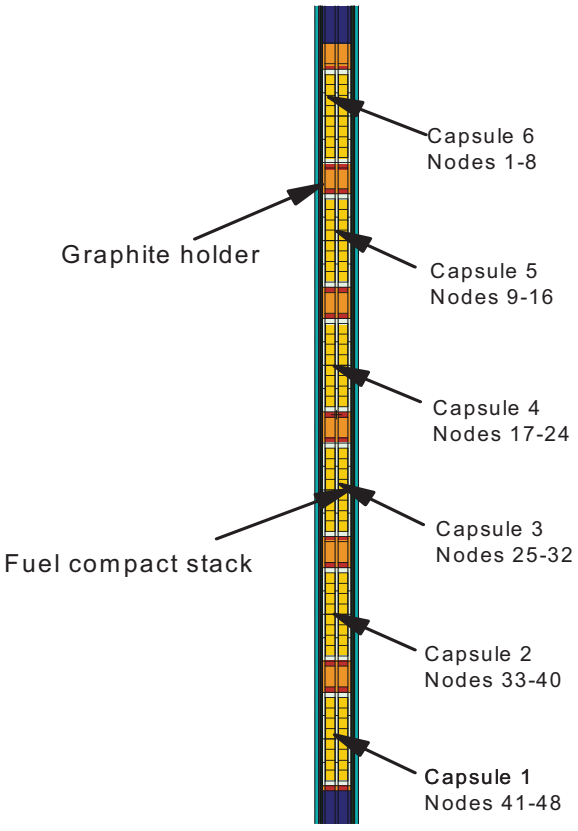

Fig 3. Axial cross-section view of the six capsules in an AGR-1 experiment capsule assembly.

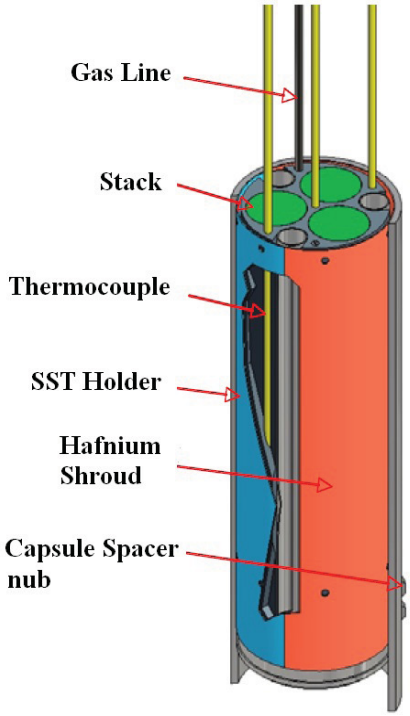

Fig 4. Three-dimensional cutaway rendering of single AGR-1 capsule.

II.A. Finite Element Mesh

Fig 5 shows the finite element mesh with a cutaway view of the entire model. A Cartesian coordinate system is appropriate for this model because of the three fuel stacks making it non-symmetric. Approximately 350,000 eight-noded hexahedral brick elements were entirely used in all the models. A set of conduction-convection elements was used to model the flow of the water. All other elements were modeled solely for diffusion heat transfer. Several mesh convergence studies have been performed on the mesh. Identical agreement for this mesh and a mesh with twice as many elements in each direction was performed. The graphite holder and fuel compacts were modeled as 0.1016 m lengths, but most of the heat comes from the fuel compacts and not from the outer components. The water is the ultimate heat sink for each capsule. The graphite holder with its two end-cap spacers and ring were modeled for the inner part of the model. A radiation boundary sink temperature of (204.4°C) is placed on the top and bottom of each graphite end cap. This value came from previous models discussed in Reference [1] for typical operating conditions.

II.B. Compact Thermal Conductivity

The fuel compact thermal conductivity was taken from correlations presented from Gontard in Reference [4] which gives correlations for conductivity, taking into account temperature, temperature of heat treatment, neutron fluence, and TRISO-coated particle packing fraction.

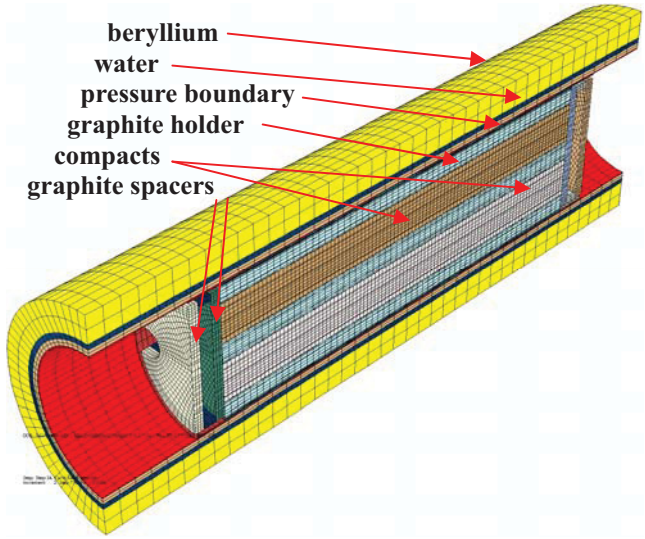

Fig 5. Sideways cutaway view of mesh with colored entities.

In this work, the convention used to quantify neutron damage to a material is fast fluence E >0.18 MeV, yet in the work by Gontard [5], the unit used was the dido nickel equivalent (DNE). In order to convert from the DNE convention to the fast fluence >0.18 MeV, the following conversion was used:

$$\Gamma_{>0.18MeV} = 1.52\ \Gamma_{DNE} \quad (1)$$

where Γ is neutron fluence in either the >0.18 MeV unit or DNE. The correlations in the report by Gontard [4] were further adjusted to account for differences in fuel compact density. The correlations were developed for a fuel compact matrix density of 1.75 g/cm^3, whereas the compact matrix used in AGR-1 had a density of approximately 1.3 g/cm^3. The thermal conductivities were scaled according to the ratio of densities (0.74) in order to correct for this difference.

Fig 6 shows a three-dimensional plot of the fuel compact thermal conductivity varying with fluence and temperature. For fluences greater than 1.0 x 10^{25} neutrons/m^2 (E > 0.18 MeV), the conductivity increases as fluence increases for higher temperatures, while the opposite occurs at lower temperatures because of the annealing of radiation-induced defects in the material with high temperatures.

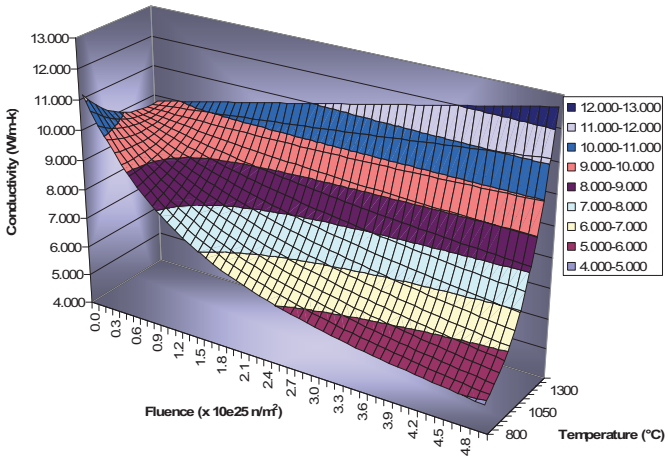

Fig 6. Three-dimensional plot of fuel compact thermal conductivity (W/m-K) varying with fluence and temperature.

II.C. Graphite Thermal Conductivity

Unirradiated graphite thermal conductivity data for the holders were provided by GrafTech [6]. Fig 7 shows unirradiated thermal conductivity of four different types of boronated graphite. The percentages indicate the weight percent (wt%) boron present in the material. The 5.5% against grain (was used in the holders for Capsules 1 and 6, while the 7% against grain was used in Capsules 2–5. The higher boron content was placed in the interior capsules (2–5) as these locations experience a greater thermal neutron flux than the two outer capsules (1 and 6) and the higher boron content provided a flatter compact heating profile through the irradiation. The against grain (AG) graphite was used and are indicated with arrows in the legend of Fig 7.

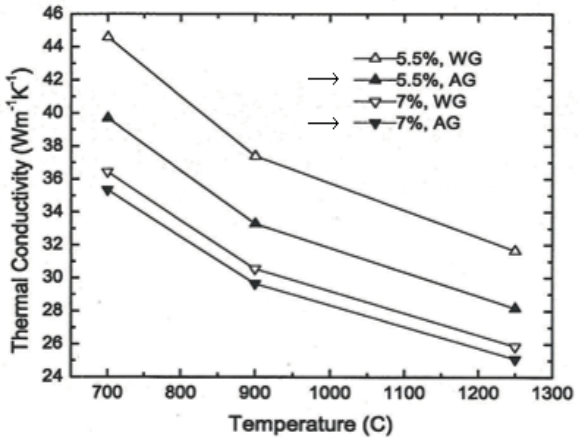

Fig 7. Thermal conductivity (W/m-K) of unirradiated, boronated graphite holders [6].

The effect of irradiation on the thermal conductivity of the graphite was accounted for in this analysis using the following correlation by Snead [7].

$$\frac{k_{irr}}{k_0} = (0.25 - 0.00017 * T_{irr}) * A * \log(dpa) + 0.000683 * T_{irr}$$
$$A = -1.0 \qquad (2)$$

where k_{irr} and k_0 are thermal conductivity of irradiated and unirradiated graphite, respectively, T_{irr} is the irradiation temperature (°C), and *dpa* is displacements per atom. The multiplier used to convert fast fluence (>0.18 MeV) to dpa is 8.23 x 10^{-26} dpa/(n/m^2) and comes from Sterbentz [8]. Fig 8 shows a three-dimensional plot of this ratio (k_{irr}/k_o) varying with dpa and temperature. The ratio of irradiated to unirradiated thermal conductivity increases for higher temperatures and decreases for higher dpa.

II.D. Gas Mixture Thermal Conductivity

Heat produced in the fuel compacts is transferred through the gas gaps surrounding the compacts into the graphite holder via a gap conductance model using the gap width and the conductivity of the sweep gas as discussed below. Since the temperature difference between the compacts and the holder is so small, no radiative heat transfer was considered across this gap. Heat is transferred across the outer sweep gas flow region between the outside of the graphite holder and the inside of the stainless-steel liner via radiation between the two surfaces and conduction through the helium/neon sweep gas. Because the thermal capacitance of the sweep gas is very low (30 cc/min), advection is not considered in the sweep gas, and it is modeled as stationary. The convective heat transfer from these sweep gases would be less than 0.01% of the heat transfer across the gap because of the low density, low flow rate, and low thermal capacitance. The thermal conductivity of the sweep gas was determined using the kinetic theory of gases used by the commercial Computational Fluid Dynamics code FLUENT [9], which gives conductivity k of a gas mixture as a function of the gas constituents i and j according to

$$k = \sum_i \frac{Y_i k_i}{\sum_j Y_j \phi_{ij}} \qquad (3)$$

where Y_i is the mole fraction of gas i, and k_i is the thermal conductivity of pure gas i.

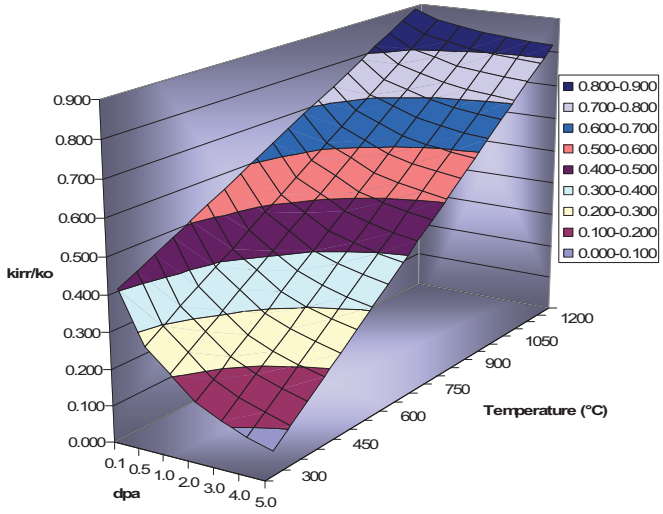

Fig 8. Graphite thermal conductivity plot of ratio of irradiated over unirradiated (k_{irr}/k_o) varying with temperature and dpa.

The parameter ϕ_{ij} in Equation 3 is given by

$$\phi_{ij} = \frac{\left[1+\left(\frac{\mu_i}{\mu_j}\right)^{1/2}\left(\frac{MW_j}{MW_i}\right)^{1/4}\right]^2}{\left[8\left(1+\frac{MW_j}{MW_i}\right)\right]^{1/2}} \quad (4)$$

where μ_i is the viscosity of pure gas i and $M_{w,i}$ is the molecular weight of pure gas i. Pure gas properties were taken from Toulukian [10]. Fig 9 shows a plot of the resulting helium/neon sweep gas thermal conductivity versus temperature and mole fraction of helium. The thermal conductivity increases as the helium mole fraction increases and as the temperature increases.

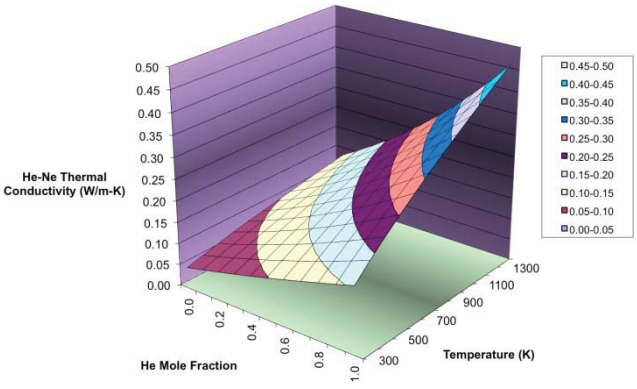

Fig 9. Sweep gas thermal conductivity versus temperature and mole fraction helium.

II.E. Conduction and Radiation Heat Transfer

The governing equation of steady-state heat transfer for the model is taken as

$$\rho c_p\left(u_x\frac{\partial T}{\partial x}+u_y\frac{\partial T}{\partial y}+u_z\frac{\partial T}{\partial z}\right)= \frac{\partial}{\partial x}\left(k(T)\frac{\partial T}{\partial x}\right)+\frac{\partial}{\partial y}\left(k(T)\frac{\partial T}{\partial y}\right)+\frac{\partial}{\partial z}\left(k(T)\frac{\partial T}{\partial z}\right)+Q \quad (5)$$

where ρ is the density, c_p is the specific heat, u_x, u_y, and u_z are the three directional velocities, T is temperature, x, y, and z are directions, $k(T)$ is the thermal conductivity varying with temperature, and Q is the heat source. The velocity of the water (u_z) was taken from Reference [1]. The gas gaps between the graphite holder and the stainless-steel-retainer sleeve used the above mentioned gas mixture conductivity correlation and were modeled with solid eight-noded brick elements with diffusion heat transfer. Approximately 80-85% of the heat transfer is by conduction, with 15-20% by radiation across the control gas gap, with less than 0.01% by advection. Ranges are given here to cover different temperatures for the fuel compacts.

Conduction heat transfer across gas gaps using the ABAQUS *Gap Conductance model was implemented on the gaps between the following surface pairs followed by gap distance: (4)

- fuel compacts and graphite holder (0.000064 m)
- bottom and top graphite spacers with stainless steel retainer sleeve (0.000965 m)
- bottom and top graphite rings with stainless steel retainer sleeve (0. 000965 m)
- graphite spacers with graphite spacers on top and bottom (0.003175 m).

The governing equation for radiation heat transfer across the gas gaps is taken as

$$q_{net} = \frac{\sigma\left(T_1^4 - T_2^4\right)}{\frac{(1-\varepsilon_1)}{\varepsilon_1 A_1}+\frac{1}{A_1 F_{12}}+\frac{(1-\varepsilon_2)}{\varepsilon_2 A_2}} \quad (6)$$

where q is the net heat flux, σ is the Stephan Boltzmann constant, T_1 and T_2 are the surface temperatures, ε_1 and ε_2 are the emissivities of Surfaces 1 and 2, A_1 and A_2 are the areas of Surfaces 1 and 2, and F_{12} is the view factor from Surface 1 to 2.

Radiation heat transfer using the ABAQUS *Gap Radiation model was implemented on the following surface pairs:

- graphite holder with stainless steel retainer sleeve
- graphite holder with thru tubes
- thru tubes with stainless steel retainer sleeve
- bottom and top graphite spacers with stainless steel retainer sleeve
- bottom and top graphite rings with stainless steel retainer sleeve

- graphite spacers with graphite spacers on top and bottom.

Radiation heat transfer was not considered between the compact surfaces and the graphite holder. This assumption was made since there appears to be about 5-10°C temperature difference between the surfaces. If the radiation would have been included, it would lower the compact temperatures by 1-2°C (almost negligible). A surface radiation boundary condition using the ABAQUS *Surface Radiation model was placed on the top of the top graphite spacer and the bottom of the bottom graphite spacer and radiated to an infinite medium of (204.4°C). In order to calibrate the finite element thermal model, the emissivities of the outer surface of the graphite holder and the inner surface of the stainless-steel sleeve were adjusted such that predicted and measured thermocouple (TC) temperatures agreed as closely as possible early in the irradiation before TC drift had become important. View factors for each surface pair were set at 1.0. An emissivity value of 1.0 for all surfaces gave best agreement between calculation and measurements. In fact, during assembly of the test, the presence of graphite dust was noted on these surfaces, which would serve to raise the emissivities of these surfaces to values closer to their maximum possible value of 1.0. Inspection of the test train during post-irradiation examination showed black surfaces on the stainless steel.

II.F. Daily Gas Mixtures

Neon fraction for each day was calculated for each capsule using average daily flow rates for Helium and Neon.

II.G. Neutron Fluence

Graphite and fuel compact material properties vary with neutron fluence. Fluence was imported from the detailed physics daily as-run calculations in Reference [4]. Fluence was taken as Field Variable 2 in the ABAQUS input model, while the neon fraction was taken as Field Variable 1.

II.H. Component Heat Rates

The gamma/neutron heating for the various components (including the fuel compacts) were taken from the as-run physics calculations in Reference [4]. Figure 10 shows the graphite heat rates averaged for each capsule varying with time of irradiation. The heat rate decreases in time with time due to the damage of the neutrons in the graphite because of the Boron-10 depletion. The components on the inside of the water had the greatest effect on the temperature of the fuel compacts.

II.I. Fuel Compact Heat Rates

Figure 11 shows the as-run physics analysis heat rates for the fuel compacts varying with irradiation time (EFPD). As the Boron-10 in the graphite burns out, the fuel compacts reach their maximum heat rates about 40% of the way through the experiment at 250 EFPDs. An EFPD for the ATR is considered a full day at full normal operating power. Capsules 3 and 4 have the highest heat rates due to the traditional chopped cosine power profile of the ATR.

II.J. Gas Gaps Changing Linearly with Time

The control gas gaps and the compact-graphite holder gas gaps were modeled as changing linearly with time. This was accomplished by having the gap conductivity of each capsule change with neutron fluence. Fluence was set as Field Variable 2 in the ABAQUS model. The original finite element mesh models created in ABAQUS were done with the as-built dimensions for the gas gaps. PIE measurements were used as the final gas gaps. The gas gaps were assumed to be the hot gas gap dimension, the hot gas gap dimension and room temperature gas gap dimension being virtually the same. Table I shows the starting and ending gas gap dimensions for the control gas gap and the compact-graphite holder gas gap. The graphite holder might be experiencing irradiation swelling, causing the compact-holder gap to increase and the control gap to decrease. Capsules 1 and 6 have 5.5% B4C, while capsules 2-5 have 7.0% B4C. The smaller amount in capsules 1 and 6 appear to have the final affect of shrinking the holder (larger gas gap), while capsules 2-5 appear to have enough B4C to swell and increase the holder (shrink the gap) as noted in Reference [11]. The gas mixture conductivity for the control gas gap was ratioed by the original model gap compared to the time varying gap. This was also done for the gap between the compacts and holder that use the "gap conductance" model in ABAQUS. Table I also shows the final fluence for each capsule.

Table I

Gas gap dimensions varying by capsule and time.

Capsule #	Control Gap Start (mm)	Control Gap End (mm)	Compact – Holder Gap Start (mm)	Compact –Holder Gap End (mm)	Ending Fluence ($x10^{25}$) (n/m^2)
6	0.716	0.782	0.064	0.168	2.56
5	0.358	0.155	0.064	0.168	3.37
4	0.254	0.127	0.064	0.165	3.78
3	0.236	0.119	0.064	0.165	3.82
2	0.279	0.102	0.064	0.157	3.54
1	0.457	0.551	0.064	0.089	2.86

III. RESULTS

Figures 12 through 16 show the results of the daily as-run thermal analysis for the AGR-1 experiment.

III.A. General Temperature Results

Figure 12 shows a cutaway view of the temperature contour plot of the graphite holder at about 40% of the way through irradiation. The hottest region occurs in the very center of the holder. Figure 13 shows a cutaway view of the three fuel compact stacks. Temperatures range from 802°C to a maximum of 1256°C. Stacks 1 and 3 have higher temperatures than Stack 2 because they are closer to the core center at this point in the irradiation. At the end of irradiation, stack 2 has higher heat rates since its fuel is not as depleted as stacks 1 and 3. The following equation was used to calculate the capsule average fuel temperatures:

$$T_{ave} = \frac{\sum T_i V_i}{\sum V_i} \tag{7}$$

where T_{ave} is the average capsule temperature, T_i is the finite element average temperature from each fuel compact finite element in ABAQUS, and V_i is each finite element volume from ABAQUS. Figure 14 shows daily average TC measured and predicted temperatures for the 625 EFPDs during the 13 reactor cycles. A moderately good agreement occurs between the measured and predicted TC temperatures (within 5-10%). The possibility exists that the TCs are drifting due to various factors including neutron bombardment as shown with the measured TC1 in capsule 6. After the first three cycles, the TCs failed for the lower three capsules, so no comparisons can be made.

III.B. Time Average Volume Average Temperature Results

Figure15 shows the calculated time average-volume average (TAVA) fuel temperatures for Capsules 6 through 1 for all fuel compacts at the very end of irradiation. Since TCs were placed in the graphite holder and not in the fuel compacts, measured TAVA values for fuel were not available. The time average-volume average value is described as

$$TAVA = \frac{\sum T_{ave,i} \Delta t_i}{\sum \Delta t_i} \tag{8}$$

where *TAVA* is the time average-volume average capsule temperature, $T_{ave,i}$ is described in Equation 7, and Δt_i is the time difference from one time-step to the next.

These final values (end of irradiation) of TAVA will be useful when doing PIE of the AGR-1 experiment. Figure 15 also shows that the final *TAVA* for capsules 6 through 4 has a peak on the third compact, while capsules 3 through 1 has a peak on the second compact. This is due to the heat generation rate in the ATR core that is shaped like a chopped cosine curve.

III.C. Comparison between Normalized Volume Average Fuel Temperature and Log of R/B for Radionuclide Kr-85m

Since there was no fuel particle failure, the radionuclide release-to-birth ratios (R/Bs) are believed to closely follow capsule fuel temperature over time. Therefore comparison between fuel temperature and R/B will help to demonstrate that the calculated capsule fuel temperatures correctly reflect the capsule thermal condition. First, the volume average fuel temperature (T_{Nor}) and log of R/B for Kr-85m radionuclide ($Log(R/B)_{Nor}$) are normalized as in following formula for fuel temperatures:

$$T_{norm,i} = \frac{T_i - \left(T_{ave,i} - T_{-2\sigma}\right)}{T_{+2\sigma} - T_{2\sigma}} \tag{9}$$

where $T_{norm,\,i}$ is the normalized daily temperature, T_i is the daily capsule average temperature, $T_{2\sigma}$ is two standard deviations, and $T_{ave,i}$ is the capsule average over all the entire irradiation. Equation 8 is also used to normalize the log (R/B).

To increase comparison accuracy, all data from the following conditions are excluded: ATR less-than-full power period, cool capsule conditions, and uncertain R/B value (too low) because of instrument measurement threshold. Thus, before the normalization for both parameters, filtering was done on the data as follows:

- AGR-1 run on pure helium during the first cycle
- Power less than 20 MW (during ATR power-up or -down period)
- Log R/B for Kr-85m less than -10
- Simulated TC-1 less than 600°C (to exclude all data from cool capsule conditions).

More filtering was done to exclude all normalized values that are below 0.0 as outliners.

Figure 16 shows the difference between the normalized temperature and the normalized log (R/B) with linear fits for four different zones of EFPDs. These four zones were chosen as they seemed to fit natural trends in the differences. It is hard to say why these definite trends exist. Capsules 3 and 2 are very similar. It appears that both differences are linearly increasing during the Zone 4 period that covers the last three operating cycles.

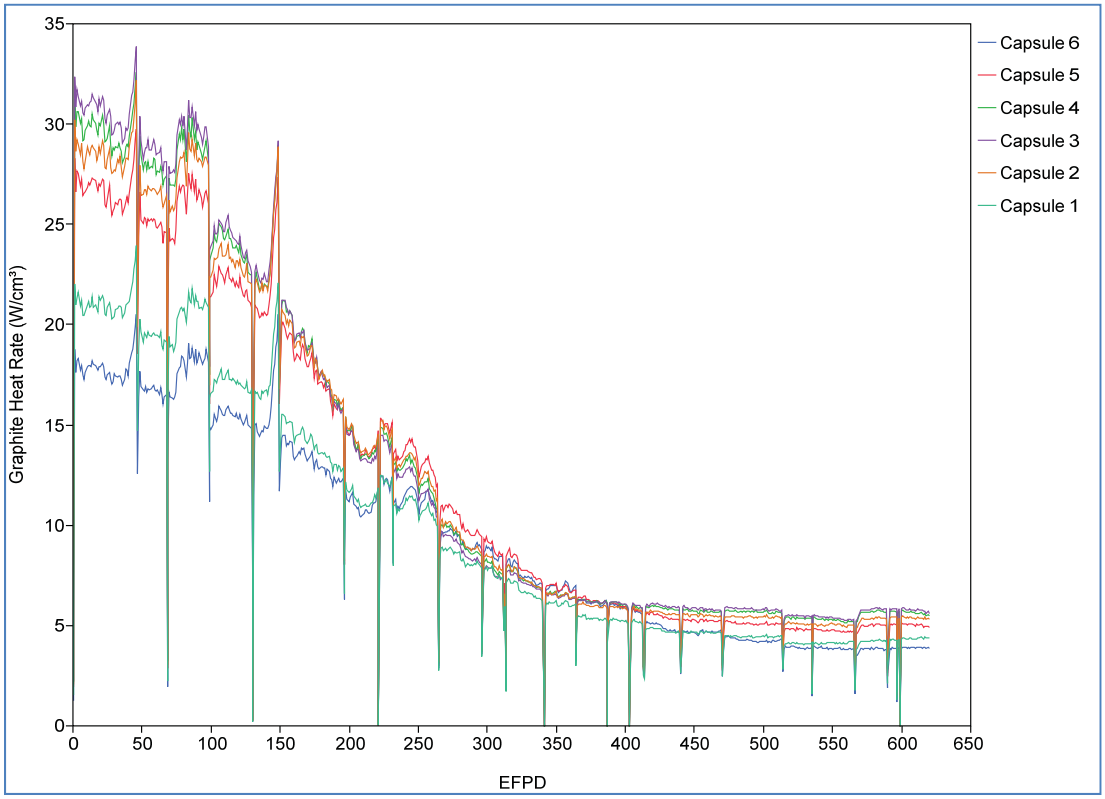

Fig 10. Daily graphite heat rates versus EFPD.

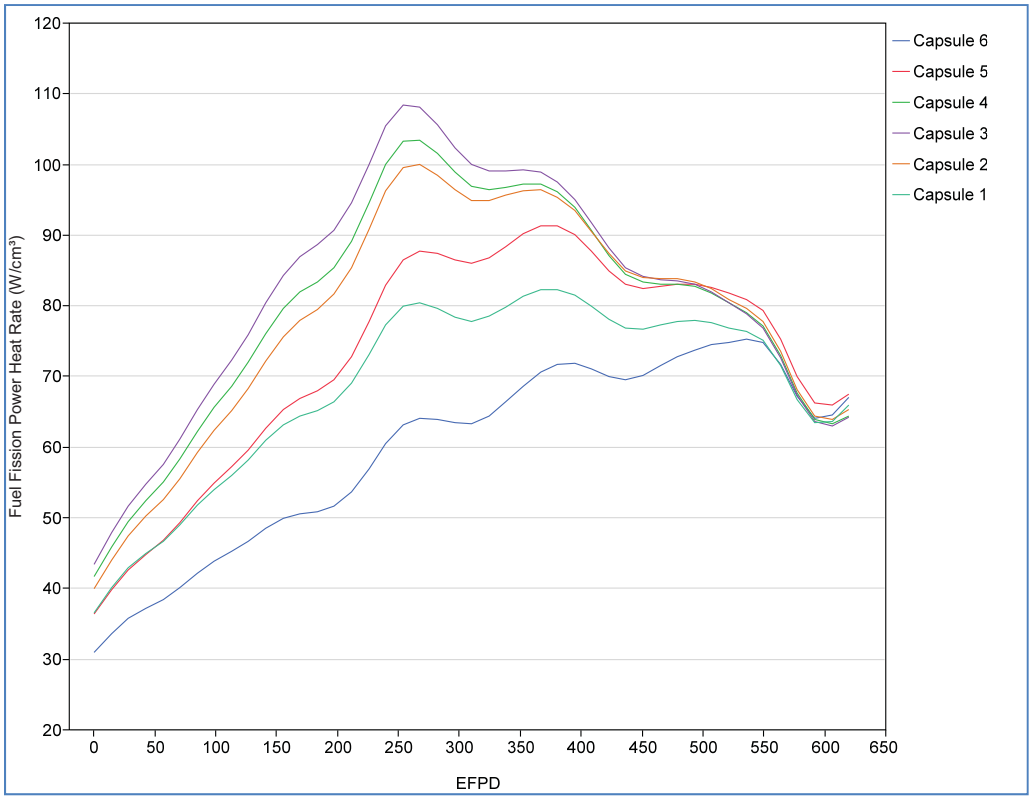

Fig 11. Smooth plot of daily capsule average volumetric heat rates in compacts versus EFPD.

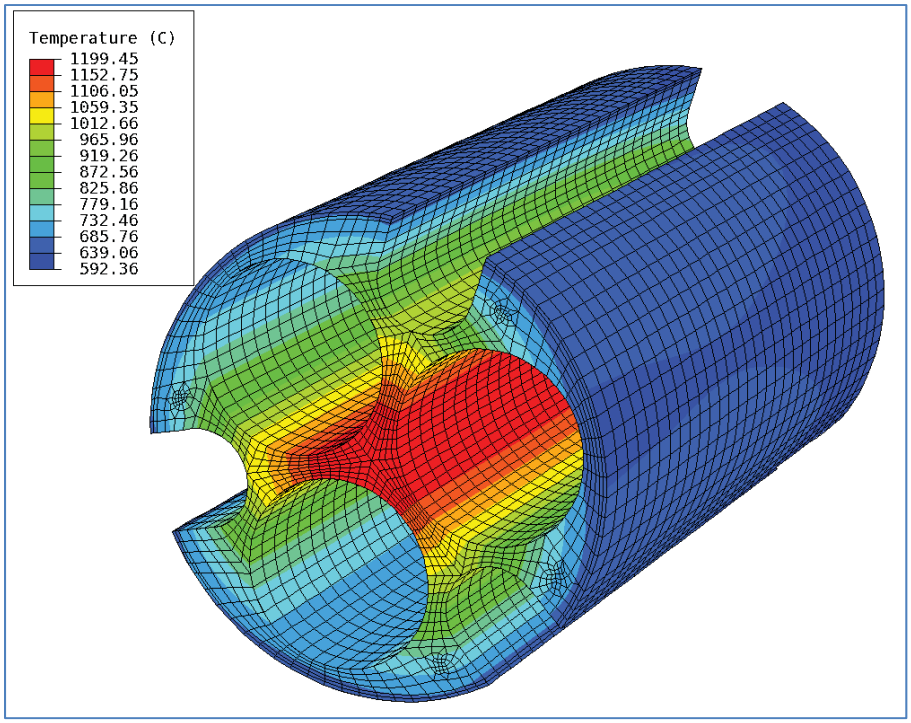

Fig 12. Temperature (°C) contour plot of cutaway view of graphite holder for capsule 4.

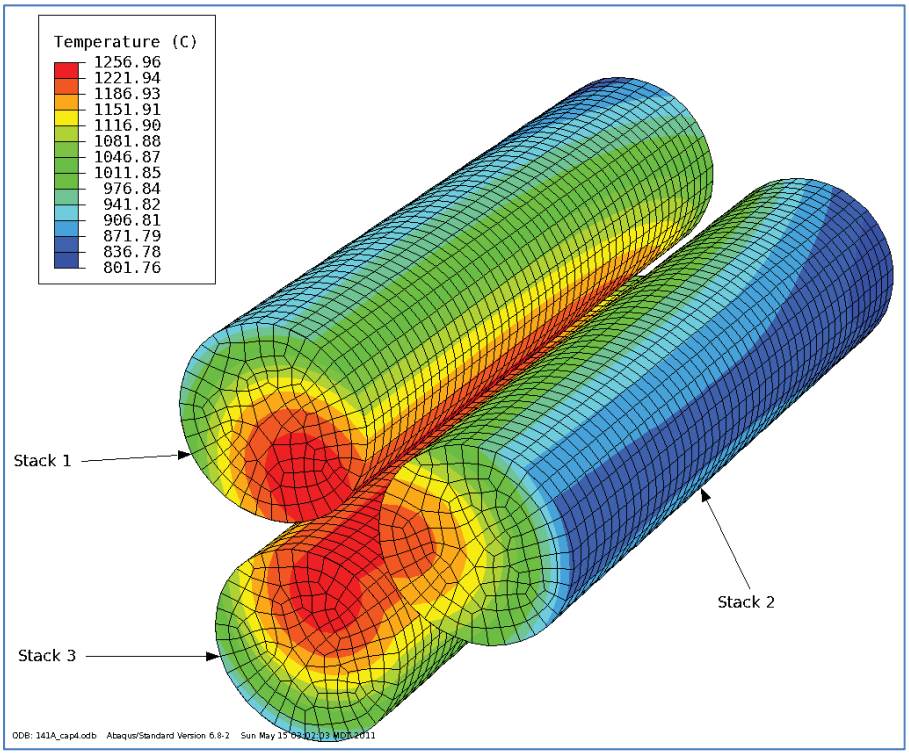

Figure 13. Temperature (°C) contour plot of cutaway view of three fuel stacks for capsule 4.

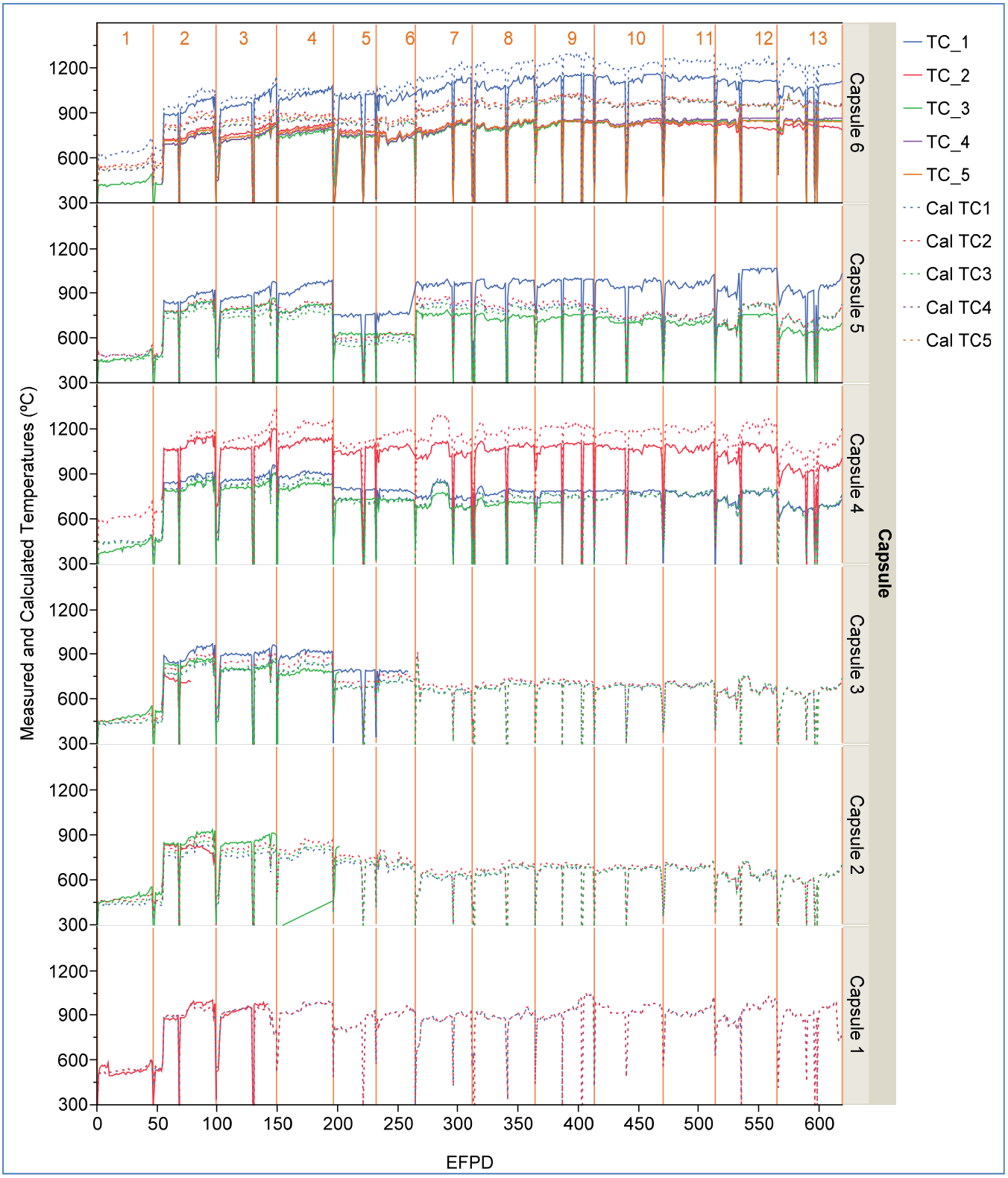

Fig 14. Measured and predicted TC temperatures.

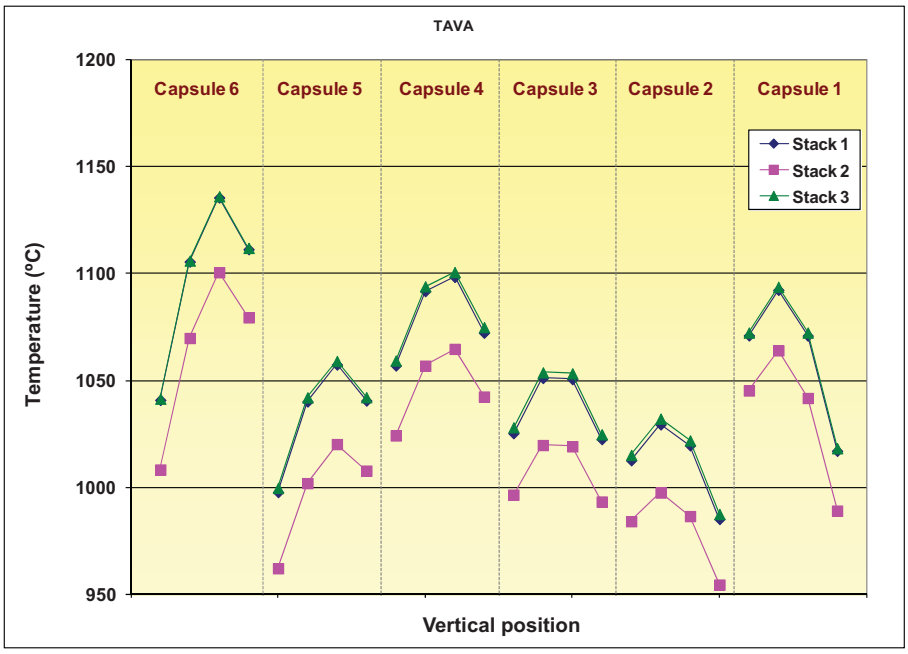

Fig 15. Calculated time average volume average temperatures for fuel Compacts 1 through 4 for all stacks and all capsules at the very end of irradiation.

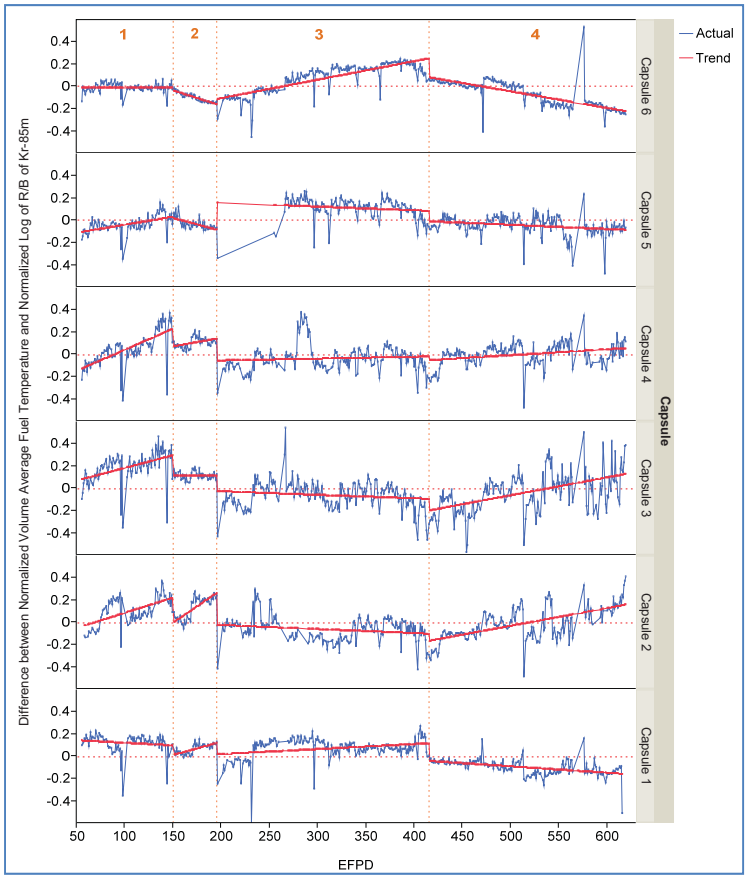

Fig 16. Difference between normalized volume average fuel temperatures and normalized log of Kr-85m R/B as a function of EFPD with linear projections.

IV. CONCLUSIONS

A daily as-run thermal analysis has been performed for the AGR-1 fuel experiment for all six capsules during the entire irradiation of the experiment. A finite element heat transfer model was created to simulate this experiment. Heat rates and fluence were imported from a daily as-run detailed physics analysis. Thermal conductivity of the fuel compacts and graphite holders varied with fluence and temperature. Boron content in the graphite holders varied with position in the core. Control gas gaps and compact-graphite holder gas gaps were implemented as varying with time. The gaps changed linearly with time starting with the as-fabricated gaps to the gaps measured after irradiation. Comparisons with actual TC measurements show a moderately good correlation with the thermal predictions that are within 5-10%. Temperatures and log (R/B) were normalized and compared with each other. A very good correlation was shown to exist between these two calculated parameters.

ACKNOWLEDGMENT

Work supported by the U.S. Department of Energy, NGNP Program, Idaho Operations Office Contract DE-AC07-05ID14517.

REFERENCES

1. G.L. Hawkes, et. al., "*Daily Thermal Results of the AGR-1 Experiment in the Advanced Test Reactor*," paper # 1039, ANS Annual Conference, San Diego, CA, June 2010.

2. G.L. Hawkes, et. al., "*Sensitivity Evaluation of the Daily Thermal Predictions of the AGR-1 Experiment in the Advanced Test Reactor*," paper # 11186, ICAPP 2011 Conference, May 2011, Nice, France.

3. Dassault Systèmes, ABAQUS Version 6.8-2, www.simulia.com or www.abaqus.com, Providence, Rhode Island, 2007.

4. J. W. Sterbentz, et. al., "*Monte Carlo Depletion Calculation for the AGR-1 TRISO Particle Irradiation Test*," paper # 1308, ANS Annual Conference, San Diego, CA, June 2010

5. R. Gontard and H. Nabielek, "*Performance Evaluation of Modern HTR TRISO Fuels*," Forschungszentrum Jülich GmbH, HTA-IB-05/90, July 31, 1990.

6. T. L. Thompson, Letter from GrafTech to the Idaho National Laboratory, July 13, 2006.

7. L. L. Snead and T. D. Burchell, "Reduction in Thermal Conductivity Due to Neutron Irradiation, *22nd Biennial Conference on Carbon*, Extended Abstracts (1995) 774-775.

8. J. W. Sterbentz, "Fast Flux to DPA Multiplier," E-mail communication to G.L. Hawkes, August 5, 2009.

9. Fluent Inc., "Fluent 6.3 User's Guide," Lebanon, NH, September 2006.

10. Y. S. Touloukian, "Thermophysical Properties of Matter, Volume 3 – Thermal Conductivity," Thermophysical Properties Research Center, Purdue University, 1977.

11. P. A. Demkowicz, et. al., *AGR-1 Irradiated Test Train Preliminary Inspection and Disassembly First Look*, INL/EXT-10-20722, January 2011.